Acta Biochim Biophys Sin 2022, 54(10): 1497–1506
https://doi.org/10.3724/abbs.2022145
Advance Access Publication Date: 18 October 2022
Original Article

Original Article

An improved cell line-derived xenograft humanized mouse model for evaluation of PD-1/PD-L1 blocker BMS202-induced immune responses in colorectal cancer

Pengzhao Shang[1,†], Liting Yu[3,†], Shucheng Cao[4], Changying Guo[1,*], and Wanheng Zhang[2,*]

[1]School of Life Science and Technology, China Pharmaceutical University, Nanjing 210009, China, [2]Department of Pharmacy, the First Affiliated Hospital, and College of Clinical Medicine of Henan University of Science and Technology, Luoyang 471003, China, [3]Department of Pharmacy, Binzhou Medical University, Yantai 264003, China, and [4]School of Engineering, China Pharmaceutical University, Nanjing 210009, China
[†]These authors contributed equally to this work.
*Correspondence address. Tel: +86-15737957481; E-mail: zhangwanheng9@gmail.com (W.Z.) / Tel: +86-18252099426; E-mail: guocha@cpu.edu.cn (C.G.)

Received 26 December 2021 Accepted 13 April 2022

Abstract

The establishment of an *in vivo* mouse model mimicking human tumor-immune environments provides a promising platform for immunotherapy assessment, drug discovery and clinical decision guidance. To this end, we construct humanized NCG mice by transplanting human hCD34$^+$ hematopoietic progenitors into non-obese diabetic (NOD) Cg-*Prkdc*^{scid}*IL2rg*^{tm1Wjl}/Sz (null; NCG) mice and monitoring the development of human hematopoietic and immune systems (Hu-NCG). The cell line-derived xenograft (CDX) Hu-NCG mouse models are set up to assess the outcome of immunotherapy mediated by the small molecule BMS202. As a PD-1/PD-L1 blocker, BMS202 shows satisfactory antitumour efficacy in the HCT116 and SW480 xenograft Hu-NCG mouse models. Mechanistically, BMS202 exerts antitumour efficacy by improving the tumor microenvironment and enhancing the infiltration of hCD8$^+$ T cells and the release of hIFNγ in tumor tissue. Thus, tumor-bearing Hu-NCG mice are a suitable and important *in vivo* model for preclinical study, particularly in cancer immunotherapy.

Key words BMS202, cancer immunotherapy, cell-derived xenograft, humanized mouse model, PD-1/PD-L1 blocker

Introduction

Cancer immunotherapy is currently the most rapidly advancing field of clinical oncology. It has boosted a variety of progressive treatments for malignancies [1,2], such as immune checkpoint blockade, cancer vaccines, and chimeric antigen receptor (CAR) T-cell therapy [3,4]. However, the low response rate and inevitable side effects limit the benefits of these treatments in patients, which prompt scientists to develop novel and effective drugs or strategies for immunotherapy. A large proportion of drug candidates have been successfully validated in preclinical systems but failed in clinical trials. It is mostly attributed to differences in innate and adaptive immune systems between humans and mice, which behave distinctly in cell development, activation, and response to antigen challenges [5,6]. It is urgent to develop more immunocompetent mouse models that simulate human disease or immune response to substitute conventional experimental models to assess the efficacies of novel cancer immunotherapies in parallel with early-phase clinical human investigation.

The preclinical tumor models mainly include syngeneic mouse models, genetically engineered mouse models, patient-derived xenograft mouse models and humanized mouse models. The first-line model to evaluate immunotherapy is currently the syngeneic mouse model. It is easily manipulated, reproducible and has no host breeding requirement, however it lacks a human tumor microenvironment, heterogeneity and immunity [7]. Genetically engineered mouse models incorporate genomic instability, provide a native tumor microenvironment and reflect the tumor development process. However, challenges such as breeding challenges and variability in penetrance limit their further application [8]. The human xenograft model, characterized by implantation of human cell lines into athymic nude or severe combined immunodeficiency (SCID) mice, is one of the earliest models for assessing chemotherapy drugs in cancer treatment [9]. They simulate the complexity of human diseases and do not require a human immune microenvironment.

Athymic nude mice are widely used in immunology research. The murine strain with spontaneous deletion of the *Foxn1* gene has a missed thymus, resulting in suppression of the immune system and a decrease in the number of T cells [10]. Its immune response mainly depends on natural killer (NK) cells, neutrophils, dendritic cells and B cells.

Establishing a new PDX model that faithfully mirrors the tumor immune microenvironment is of significance. At present, researchers have constructed humanized mice by engrafting cultured $CD34^+$ HSCs or cultured precursor cells (HSPCs) [11–14]. Implanting human peripheral blood mononuclear cells (PBMCs) is also an available option [15,16]. However, the time period of PBMCs remaining viable after engraftment limits their further application [17]. Therefore, PBMCs are unsuitable for examining immune responses *in vivo*, such as immune checkpoint blocker action. To better reshape the human immune system in mice, we developed a humanized mouse model by implanting human $CD34^+$ stem cells from cord blood to irradiated NCG mice to recapitulate the human immune system in NCG mice.

It has been reported that NCG mice reconstituted with umbilical cord human $CD34^+$ cells induces transplanted human PDX tumors to regress after anti-PD-1 treatment [18]. Additionally, pembrolizumab (anti-PD-1 mAbs) showed a significant growth inhibition effect in several cell line-derived xenografts (CDXs) and PDX tumors in Hu-NCG cells. However, it does not work in non-small cell lung cancer (NSCLC), sarcoma, bladder cancer, and triple-negative breast cancer (TNBC) of NCG mice [19]. There is evidence that cytotoxic $hCD8^+$ T cells play a vital role in inhibiting tumor growth [19]. Currently, although tumor-bearing Hu-NCG mice have been used as a platform for preclinical immunotherapy research on different types of tumors, their application in colorectal cancer research has not yet been reported. Furthermore, mAbs are the most commonly applied PD-1/PD-L1 blockers in the treatment of different malignancies in clinical practice [20]. However, due to the inevitable drawbacks of antibodies, such as long half-life, adverse events induced by immune response and poor permeability, it is necessary to develop small-molecule blockers. BMS202 acts as a small molecule blocker that binds to human PD-L1 and blocks its interaction with PD-L1. It has been verified to have low toxicity towards cell lines *in vitro*. To date, there have been no reports on hu-NCG colorectal cancer mouse models for the evaluation of BMS202 and other small molecules.

In the present study, we successfully rebuilt the human immune system in NCG mice and monitored immune cell development at different time points (functional T and B lymphocytes and NK cells). Meanwhile, the implantation of human colorectal CDXs into humanized mice was established. The small molecule PD-1/PD-L1 checkpoint blocker BMS202 showed good antitumour responses in a hu-NCG colorectal cancer mouse model. Thus, this improved CDX humanized mouse model represents an effective method for assessing small molecules for immune checkpoint blockade, which facilitates the advancement of preclinical immunotherapy research.

Materials and Methods

Mice and HSCs used for humanization

NCG (NOD/scid, IL-2Rγ^{null}) mice were purchased from Gem Pharmatech Co., Ltd. (Nanjing, China). The 4- to 5-week-old female mice used were fed in a specific pathogen-free (SPF) environment. All animal experiments were conducted following the Guidelines for Care and Use of Laboratory animals issued by the Ministry of Health of the China (No. 55, 2001) and in accordance with the Provision and General Recommendation of Chinese Experimental Animals Administration Legislation and approved by the Science and Technology Department of Jiangsu Province, China [SYXK (SU) 2016e0011]. HSCs were purchased from Novo Biotechnology Co., Ltd (Beijing, China).

Humanized NCG mice

Four- to five-week-old female mice were irradiated using a ^{137}Cs gamma irradiator with 150 cGy. The effect of the irradiator was detected by the proportion of mouse CD45 and mouse CD117. Twenty-four hours after irradiation, approximately 1×10^5 $CD34^+$ HSCs (> 90% purity) were injected into mice. Flow cytometry was used to detect the engraftment levels of human $CD34^+$ HSCs and human immune cell populations differentiated from $CD34^+$ HSCs in different organs and tissues. Five mice in each group were detected. Mice were regarded as humanized (Hu-NCG mice) when the percent of human $CD45^+$ cells in the peripheral blood was over 25%. Humanization was confirmed in all Hu-NCG mice before tumor xenograft implantation.

Establishment of humanized CRC xenograft tumors

SW480 and HCT116 cells (human colorectal cancer cell lines) were obtained from the Cell Bank of the Chinese Academy of Sciences (Shanghai, China). Both cell lines were cultured in DMEM (Gibco, Carlsbad, USA) and tested negative for mycoplasma prior to use in experiments. Humanized colorectal cancer xenograft NCG models were established by subcutaneously injecting HCT116 cells and SW480 cells (5×10^6) into Hu-NCG mice. Five mice in each group were used in the model. Tumor volumes were calculated using the formula: $V = LW^2/2$ (L: longer diameter of tumor, and W: shorter diameter of vertical direction).

In vivo experimental model of humanized colorectal cancer

Approximately two weeks after the implantation of HCT116 and SW480 cells into Hu-NCG mice, the average tumor volume reached approximately 50 mm^3. Hu-NCG mice bearing tumors were then randomized into experimental and control groups with five mice per group. Mice were administered with BMS202 (60 mg/kg, 0.1 mL/10 g) by oral gavage twice daily as previously described [21]. BMS202 was purchased from MedChemExpress (HY-19745; Monmouth Junction, USA). The tumor volumes were monitored during the treatment period. On the 35th day, the mice were sacrificed, and the tumor masses were harvested for subsequent experiments.

Flow cytometric analysis of immune cells in the blood, spleen, and bone marrow

The erythrocytes (peripheral blood, spleen, and bone marrow) were lysed with ACK Lysis buffer (Sangon Biotech, Shanghai, China). The remaining cells were washed with PBS solution and filtered through a 70 μM cell strainer. Afterwards, the cells were resuspended in PBS solution and filtered into a single-cell suspension. To evaluate the immune response after treatment, a multicolor flow cytometry panel was used to detect the changes in immune cells. First, the single cells were stained with the BD Horizon Fixable Viability Stain 700 (FVS700) (BD, Franklin Lakes, USA) to distinguish alive and dead cells for further analysis. Then, the cell

surface antigens were labelled with corresponding antibodies, such as anti-hCD45 (304035; Biolegend, Beijing, China), anti-hCD3 (300405; Biolegend), anti-hCD4 (317413; Biolegend), anti-hCD8 (300923; Biolegend), and anti-hCD25 (302609; Biolegend). For intracellular indicator staining (IFN-γ and Foxp3), the cells were fixed with Fixation/Permeabilization Diluent (cat. 00-5223-56; Thermo Fisher Scientific, Waltham, USA) for 30 min at room temperature and washed twice with permeabilization buffer (cat. 00-8333-56; Thermo Fisher Scientific). The anti-IFN-γ antibodies (562017; BD Pharmingen, San Diego, USA) and anti-Foxp3 antibodies (560082; BD Pharmingen) were incubated with cells according to the manufacturer's instructions. After staining, the cells were washed and resuspended in PBS before flow cytometric analysis. The results were analyzed by BD FACS Diva Software.

Immunohistochemistry and immunofluorescence microscopy

For immunohistochemical (IHC) analysis of KI-67, tumor tissues were fixed with 4% paraformaldehyde (PFA; Beyotime, Shanghai, China), followed by treatment with 0.1% hydrogen peroxide (Sigma, St Louis, USA), embedding in paraffin and sectioning. The slides were blocked with 10% goat serum in PBS solution and incubated with anti-KI-67 antibody (27309-1-AP; Proteintech, Wuhan, China) overnight at 4°C in a wet box. After incubation with the secondary antibody for 2 h, the samples were treated with an ABC HRP kit (Yeasen, Shanghai, China) according to the manufacturer's instructions. Then, DAB (3,3-diaminobenzidine) HRP substrate was used before counterstaining with hematoxylin (Sigma) and dehydration.

For immunofluorescence (IF) microscopic analysis, after being blocked with 10% goat serum in PBS solution, the slides were incubated with anti-CD8 antibody (66868-1-Ig; Proteintech) or anti-IFN antibody (15365-1-AP; Proteintech), followed by incubation with AF647 fluorescently labelled secondary antibodies (4410, 4414; Cell Signaling Technology, Danvers, USA) in the dark. Samples were stained with DAPI for 15 min and mounted before image acquisition. Photomicrographs were taken with a Zeiss imaging platform (LSM980; Zeiss, Jena, Germany) and SPOT Basic software. The IHC and IF images were analyzed by Image-Pro Plus software.

Western blot analysis

The human colorectal cancer cell lines HCT116 and SW480 were stimulated with human recombinant IFNγ (Abcam, Cambridge, UK) at different concentrations to induce the overexpression of PD-L1. Cell lysates were extracted from stimulated cells and denatured by boiling. Then, the samples were separated by electrophoresis on 10%–15% SDS-polyacrylamide gels and transferred to NC membranes (Millipore, Billerica, USA). Then, protein bands were probed with anti-PD-L1 primary antibodies (ab205921; Abcam, Cambridge, UK) and HRP-linked secondary antibodies (7074; Cell Signaling Technology, Danvers, USA). These blots were detected using SignalFire™ Plus ECL Reagent (12630; Cell Signaling Technology, Danvers, USA) and analyzed using the Tianon infrared imaging system and software (Beijing, China).

Statistical analysis

Statistical analysis was conducted with GraphPad Prism software (San Diego, USA). Data are shown as the mean ± SD. Student's *t* test was used for data comparison, and $P < 0.05$ was considered as statistically significant.

Results

Successful reconstitution of the human immune system

Immune-humanized tumor-bearing mice were constructed to assess the efficacies of the small molecule PD-L1/PD-1 blocker BMS202. A schematic of mouse model establishment is shown in Figure 1A. Before transplantation, the NCG mice received 150 cGy-radiation. The myeloablative results are shown in Figure 1B,C. After irradiation, the number of mCD117$^+$ cells in peripheral blood was decreased from 1.4% to 0.5%, indicating that marrow ablation was successful.

Fresh hCD34$^+$ cells were transplanted into NCG mice within 24 h after irradiation. After transplantation, the survival rate and body weight of HSC-NCG mice and NCG mice were monitored every 2 weeks (weeks posttransplantation, wpt). The survival rate of HSC-NCG mice was 80% (Figure 2A). The body weights of HSC-NCG mice were increased during the whole process, in parallel with the NCG mice (Figure 2B).

To evaluate the progress of the HSC-NCG mouse model, the reconstitution and differentiation of human immune cells (peripheral blood, spleen, bone marrow) were detected by multicolor flow cytometry at 4 weeks, 8 weeks and 12 weeks, respectively (Figure 3). The gating strategy for flow cytometry is shown in Figure 3A. As shown in Figure 3B, at week 4, approximately 1% to 3.5% of cells were human CD45$^+$ cells in the peripheral blood. The proportion of hCD45$^+$ leukocytes in the spleen (Supplementary Figure S1A) and bone marrow (Supplementary Figure S1D) were similar to those in the peripheral blood. The proportion of hCD45$^+$ cells in the peripheral blood, spleen, and bone marrow was increased to approximately 40% at week 8 (Figure 3C and Supplementary Figure S1B,E). CD3$^+$ T cells and CD19$^+$ B cells were also detected in the peripheral blood, spleen and bone marrow. On average, 15% of the human leukocytes were CD3$^+$ T cells, and 70% were CD19$^+$ B cells in the peripheral blood (Figure 3C). In the spleen and bone marrow, CD3$^+$ T cells and CD19$^+$ B cells were slightly decreased compared with those in the peripheral blood (Supplementary Figure S1B,E). At week 12, the average percentages of hCD45$^+$ cells in the peripheral blood, spleen and bone marrow were 40%, 30% and 28%, respectively (Figure 3D and Supplementary Figure S1C,F). Moreover, CD4$^+$ T cells and CD8$^+$ T cells were found within 12 weeks post CD34$^+$ HSC engraftment, which could be used as a benchmark for assessing the efficacy of immunotherapy. Interestingly, CD16$^+$/CD56$^+$ NK cells were also detectable at this stage (Figure 3D and Supplementary Figure S1C,F). In conclusion, over 25% of hCD45$^+$ cells were detected within 12 weeks of CD34$^+$ HSC implantation.

To verify the proliferation and differentiation ability of T cells derived from Hu-NCG mice *in vitro*, we isolated T cells, stimulated them with anti-human CD3 antibody and PMA, and labelled them with CFSE. Our results showed that the reconstituted T-lymphocytes were functionally active (Supplementary Figure S2A,B). Taken together, the humanized NCG mice (Hu-NCG) were successfully established. The CD34$^+$ HSCs showed robust differentiation ability and could differentiate into immune subpopulations.

Antitumour effect of BMS202 on the colorectal cancer CDX model

The processes of generating Hu-NCG mice bearing CDX tumors and

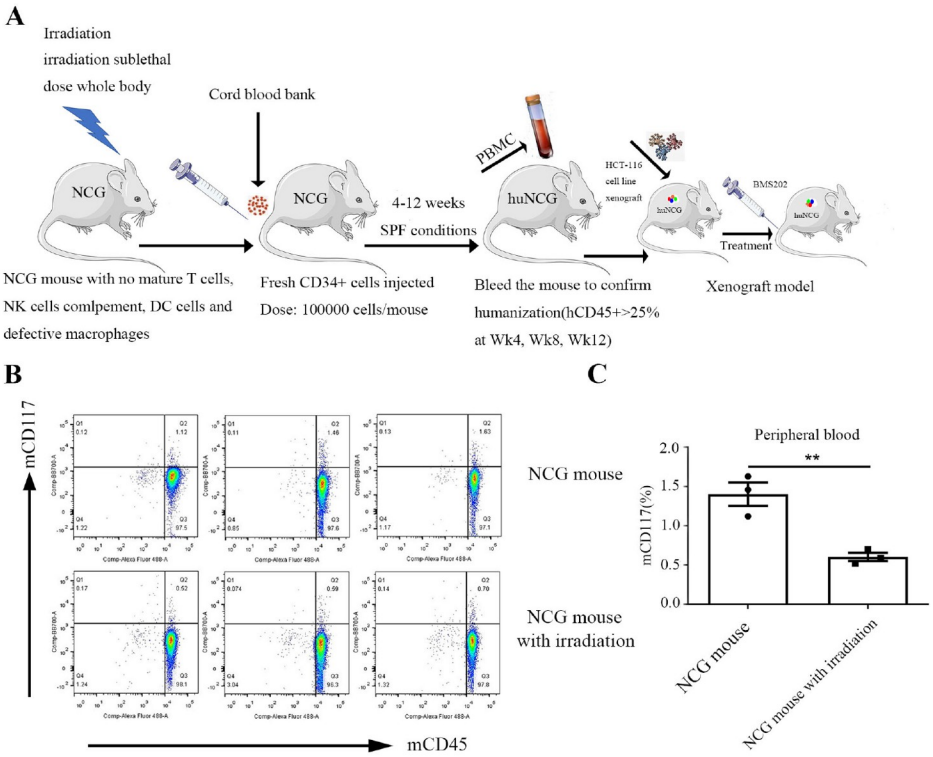

Figure 1. Illustration of establishment of the Hu-CDX mouse model (A) Graphical abstract of the establishment of the humanized mouse model. Fresh hCD34$^+$ stem cells were injected into irradiated mice *via* the tail vein. (B) Flow cytometric analysis of mouse immune cells in the peripheral blood after irradiation. (C) Comparison of the levels of mCD117$^+$ cells in NCG mice with or without irradiation.

drug administration are illustrated in Figure 2C,D. Twelve weeks later, mice had similar proportions of hCD45$^+$ cells (>25%). HCT116 and SW480 are cell lines expressing high levels of PD-L1 (Supplementary Figure S2C,D), so we implanted these two colorectal cancer cell lines into Hu-NCG mice to establish a humanized mouse model with CDX grafts. Approximately 5×10^6 HCT116 cells were inoculated subcutaneously into Hu-NCG mice. Approximately two weeks later, the tumor volume reached ~50 mm^3. Then, we assessed the PD-1/PD-L1 inhibitor BMS202 in this model.

BMS202 is a small molecule PD-1/D-L1 blocker developed by Bristol-Myers Squibb (BMS). It reduces the inhibitory effect of soluble PD-L1 on T-cell receptor-mediated T lymphocyte activation [22–24]. The HTRF binding assay results revealed that BMS202 inhibits the PD-1/PD-L1 interaction with an IC_{50} of 0.018 μM [23]. HCT116 and SW480 tumor models were chosen to evaluate the efficacy of BMS202 in the Hu-NCG CDX model. Mice were treated at 60 mg/kg with a volume of 0.1 mL/10 g by oral gavage twice a day. After 21 days of treatment, BMS202 showed a favorable antitumour effect on HCT116 tumors in the Hu-NCG model (Figure 2E–H). In the 60 mg/kg treatment group, BMS202 significantly decreased the tumor weight, and the tumor growth inhibition (TGI) value was 50% (Figure 2G,H). Meanwhile, BMS202 also displayed antitumour effects on SW480 tumors in the Hu-NCG model with a TGI value of 50% (Supplementary Figure S2E–H). In summary, BMS202 plays a crucial role in the fight against colorectal tumors in Hu-NCG mice.

BMS202-induced immune response in humanized NCG mice bearing colorectal cancer

To determine whether BMS202 treatment improves the immune response in Hu-NCG mice bearing HCT116 tumors, we examined the proportion and status of immune cells in mouse spleens. Figure 4A shows the flow cytometric gating strategy. The percentage of CD8$^+$ T cells was increased to approximately 45% in the BMS202-treated group and 30% in the control group. The ratio of CD4$^+$ T cells was similar in both groups (Figure 4B,C). As shown in Figure 4D,E, the ratio of regulatory T cells (CD4$^+$CD25$^+$Foxp3$^+$) was robustly decreased in the BMS202-treated group. Meanwhile, the number of IFNγ$^+$CD8$^+$ T cells in the BMS202-treated group was 2-fold greater than that in the control group (Figure 4F,G). Taken together, our data suggest that BMS202 activates the antitumour immune response in HCT116 tumors of Hu-NCG mice by blocking the PD-1/PD-L1 interaction.

BMS202-induced changes in the tumor microenvironment in humanized NCG mice bearing colorectal cancer

Immunofluorescence analysis was performed to determine the tumor-infiltrating lymphocytes. Compared with the control group, significantly increased infiltration of human CD8$^+$ T cells was observed in the BMS202-treated group, which was in line with the flow cytometry analysis (Figure 5C,D). The secretion of human IFN-γ was higher in the BMS202-treated tumors than in the control group (Figure 5E,F). The infiltration of CD69$^+$CD8 T cells was higher in the BMS202-treated group than in the control group (Figure 5G,H), the proportion of TIM-3$^+$CD8 T cells in BMS202-treated group was lower compared with that in the control group (Figure 5I,J). Moreover, the expression of Ki-67 in the BMS202-treated group was decreased compared with that in the control group (Figure 5A,B). The nucleus-to-cytoplasm ratios of the

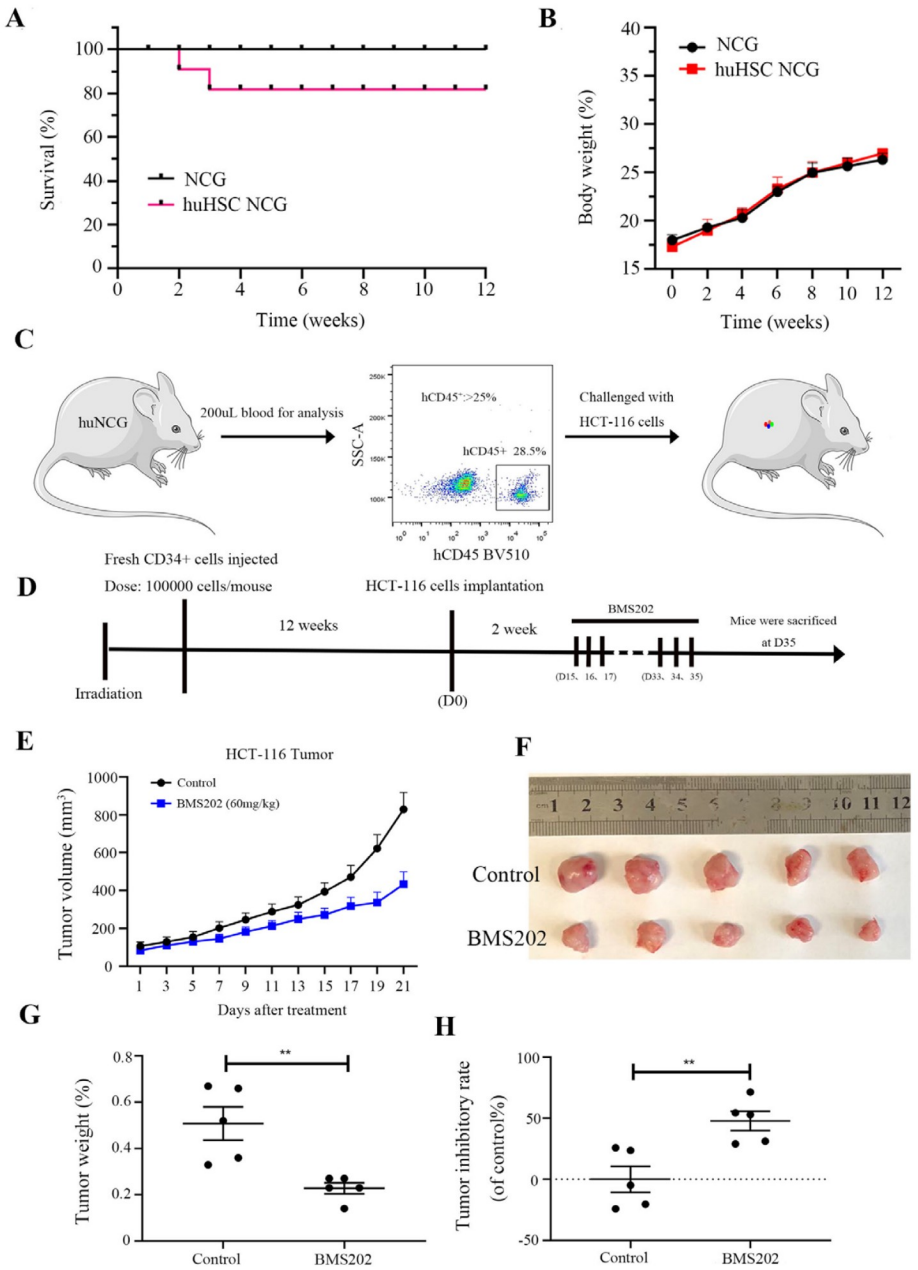

Figure 2. Antitumour activity of BMS202 in Hu-CDX cells and a human colorectal cancer model (A) Survival curves and (B) body weight changes of NCG mice and NCG mice transplanted with CD34$^+$ HSCs. (C,D) Twelve weeks after hCD34$^+$ stem cell implantation, mice were injected subcutaneously with HCT116 cells to develop the CDX model. Two weeks later, the Hu-CDX model was treated with BMS202 at 60 mg/kg twice a day for 21 days. Antitumour activity of BMS202 against HCT116 tumors in Hu-NCG mice *in vivo*. (E) Changes in tumor volume during treatment. (F) and (G) Photographs and weights of the excised tumors. (H) TGI of the treatment group. Data are presented as the mean ± SD. $^{**}P < 0.01$, $n = 5$.

treatment group were decreased based on the hematoxylin and eosin (H&E) staining results, which indicated that BMS202 inhibited tumor cell growth (Figure 5K). These data demonstrated that BMS202 increases the infiltration of hCD8$^+$ T cells and the release of hIFN-γ in humanized Hu-NCG mice bearing colorectal tumors. In other words, BMS202 activates the human immune response in this model.

Discussion

We established hCD34$^+$-derived humanized mouse models and assessed their fitness to evaluate the immunostimulatory effect of the small molecule PD-1/PD-L1 blocker BMS202. The key factor for successful establishment of a humanized mouse model is the immunodeficiency of the mouse host. Among the many immunodeficiency mouse strains available, NOD-scid IL-2Rγ^{null} (NCG) mice are currently the most widely used strain to successfully humanize the immune system with the highest transplantation rate [25–28]. After transplantation, hCD34$^+$ cells colonize the bone marrow of mice and continuously differentiate into various types of hematopoietic or immune cells, such as T cells, B cells, NK cells, and myeloid cells [19]. This model, with a stable immune reconstitution system and a long survival cycle, is an ideal model for preclinical

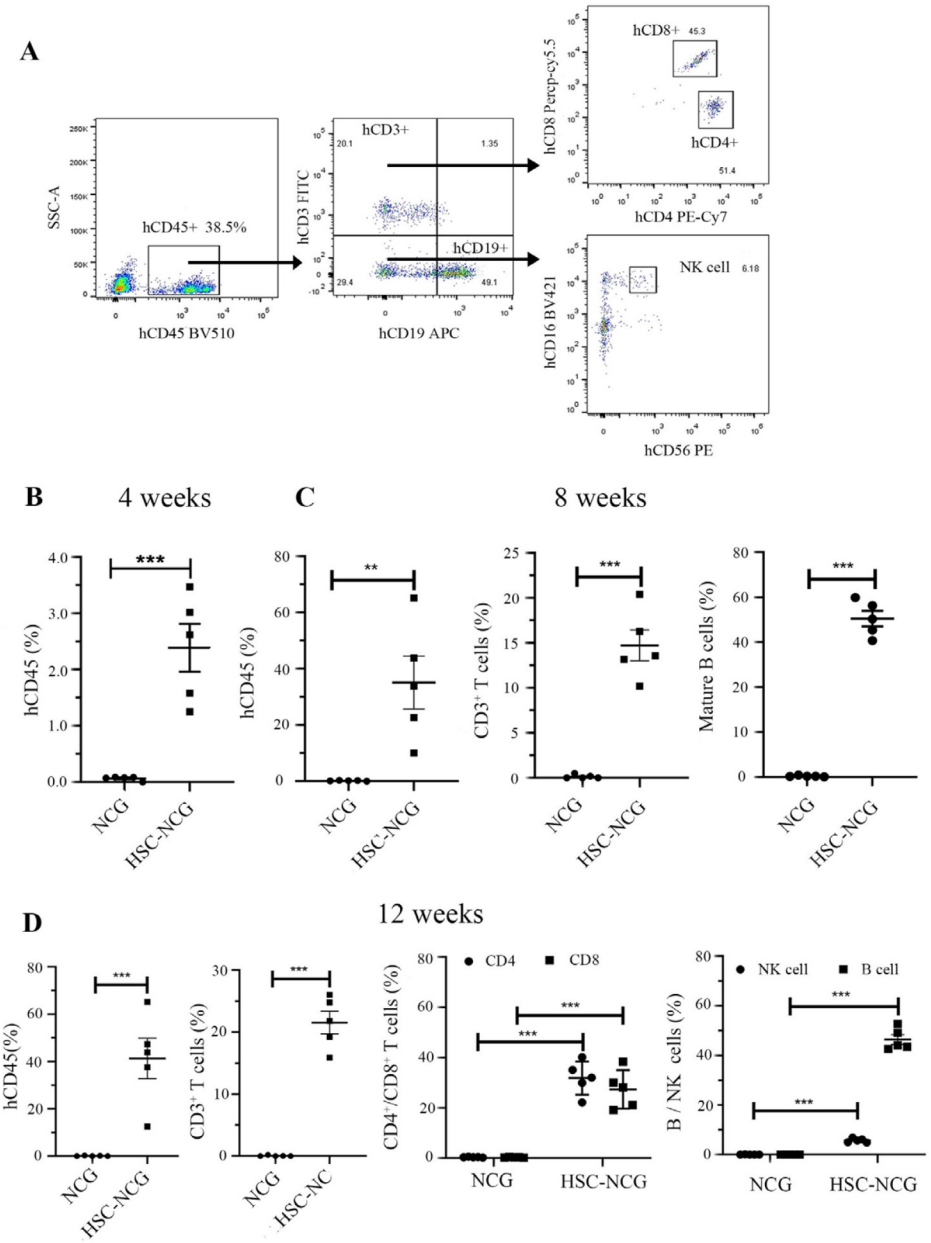

Figure 3. Monitoring the progress of the humanized mouse model by detecting human immune cells in mouse organs (A) The gating strategy of flow cytometry to detect differentiated human immune cells in mouse organs. Human CD45$^+$ lymphocytes were gated out from all cells, and human T, B, and NK cells were gated out from the human CD45$^+$ lymphocyte subpopulation. Analysis of humanization progress by human immune cells in the peripheral blood at (B) 4 weeks, (C) 8 weeks, and (D) 12 weeks after CD34$^+$ stem cell implantation. Approximately 100 μL of peripheral blood was collected for analysis. At the same time, immune analyses were performed in the peripheral blood, spleen, and bone marrow. Three independent experiments were conducted, and the results were similar. Data are presented as the mean ± SD. $^{**}P < 0.01$, $^{***}P < 0.001$, $n = 3$.

drug evaluation.

Before transplantation, myeloablization with radiation or myeloablative drugs is a necessary step [29]. The commonly used method is 150 cGy/min irradiation. In addition, busulfan is also an appropriate myeloablative drug which is suitable for use before transplantation. The traditional irradiation method was adopted in this study. However, after implantation, we found two deaths in the radiation treatment group within two weeks. This may be attributed to the radiation sensitivity of individual differences. Experiments with large samples should be exploited to confirm this inference. According to the literature, busulfan treatment resulted in a higher survival rate (approximately 80%), more effective reconstitution of human immune cells including B cells, T cells, macrophages and dendritic cells, and a longer survival time (45 weeks) of humanized NCG mice compared to total body irradiation [30–32]. In subsequent large-scale experiments, busulfan may be used as an alternative approach. After myeloablization, human CD34$^+$ HSCs were injected at a density of 1×10^5 cells/mouse via the tail vein within 24 h. Commonly, the dose of CD34$^+$ HSCs is 1×10^5 cells or higher by the intravenous transplantation method [19,33]. By bone

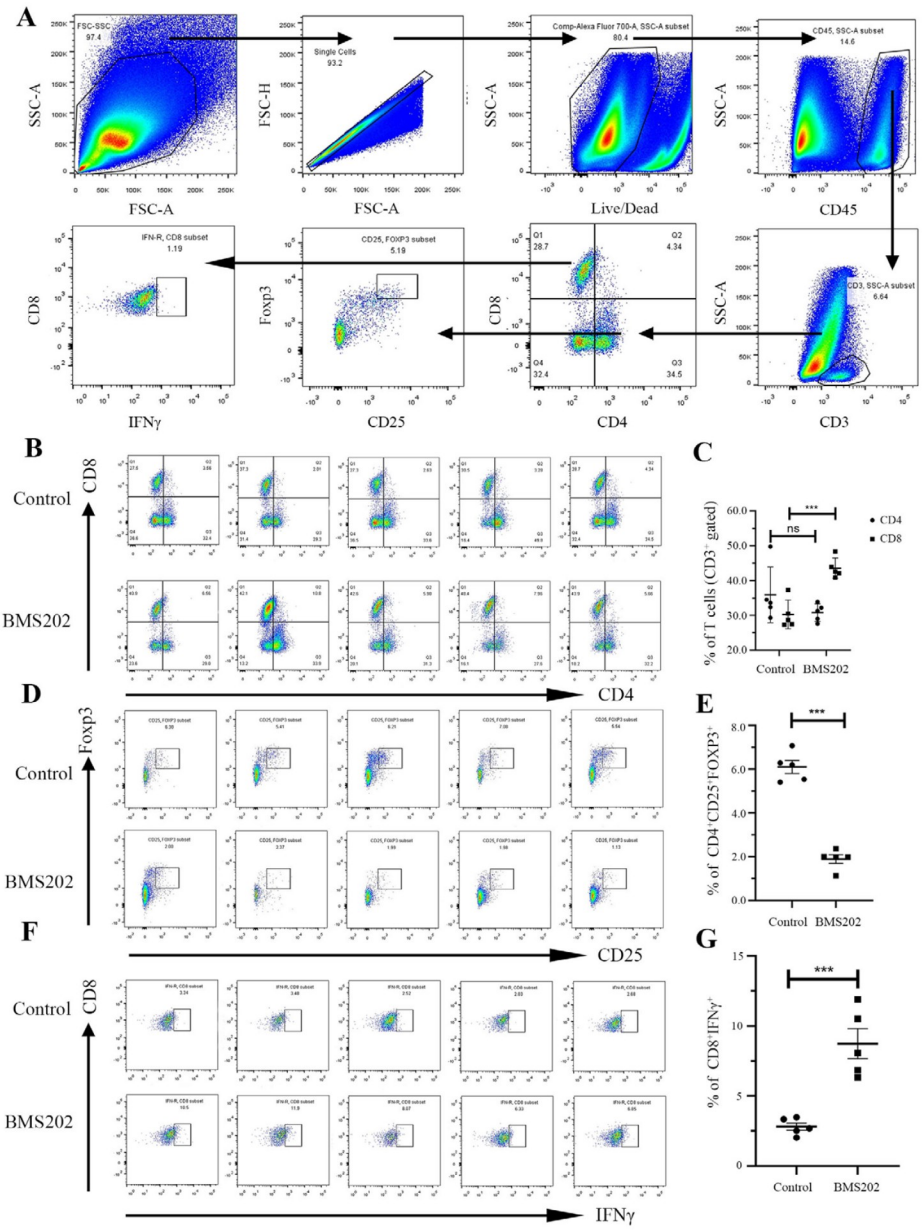

Figure 4. The antitumour immune response of BMS202 in humanized NCG mice bearing colorectal cancer (A) The gating strategy of flow cytometry for detecting human immune cells in the mouse spleen. Mouse spleens were processed into single cells and analyzed by flow cytometry, as described in the Materials and Methods. The percentages of (B) hCD4$^+$/hCD8$^+$ T cells, (D) hCD4$^+$CD25$^+$Foxp3$^+$ T cells, and (F) hCD8$^+$IFN-γ$^+$ T cells are shown. (C,E,G) Statistical analyses of these cell subsets. *P < 0.05; **P < 0.01; ***P < 0.001.

marrow transplantation, even if only 2×10^4 cells are transplanted into each mouse, a humanized mouse model can be successfully established [34,35]. Bone marrow transplantation is a more direct and efficient method with higher implantation efficiency. Different from vein transplantation, which requires blood circulation, the bone marrow transplantation method allows stem cells to enter the bone marrow microenvironment directly. It is beneficial to improve the differentiation of B cells and primary T cells and increase the number of B cells and T-cell migration to the thymus, thereby improving the reconstruction efficiency of human T and B cells.

Human CD34$^+$ HSCs differentiate into various white blood cell subgroups in NCG mice. At the 8th week, the percentage of B cells was high, while the percentage of CD3$^+$ T cells was low, which suggested that the reconstruction of T cells occurred later or slower than that of B cells. Predominant hCD19$^+$ B cells were detected, and the expression of human immunoglobulins on hCD19$^+$ B cells was also found. A significant fraction of hCD19$^+$ B cells expressed human IgM on their surface. A fraction of cells expressing IgD were also observed in the blood and spleen, suggesting that class switching occurred in these developing B cells. Therefore, class switching can effectively occur in developing B cells in NOD/SCID/IL2rγ^{null} mice [35–38]. Moreover, IgA-secreting human B cells can develop in the murine intestine, suggesting that human mucosal immunity could be generated. In summary, in the Hu-CD34$^+$HSC model, human B cells possess fundamental functions, including

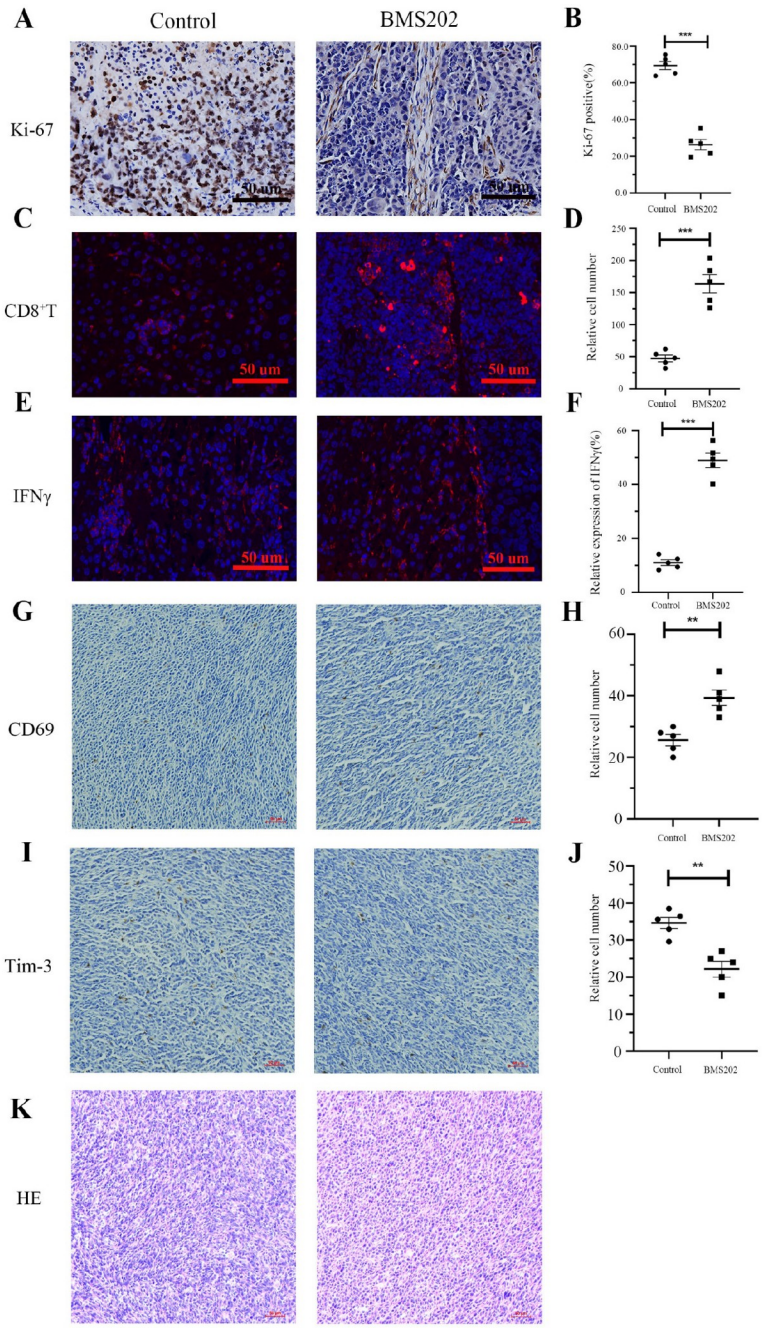

Figure 5. Comparison of the human immune microenvironment in BMS202 treated Hu-NCG mice and untreated Hu-NCG mice (A) Representative immunohistochemistry images of Ki67$^+$ tumor cells in tumor tissues. (B) Quantitative analysis of Ki67$^+$ tumor cells in both groups. The tumor cells expressing Ki-67 were counted with Image-Pro-Plus. Ki-67 positive (%) = (cell expressing Ki-67/total cells) × 100%. Immunofluorescence images for (C) CD8$^+$ T cells and (E) IFN-γ on CDX (HCT116) tissue developed in humanized mice. Quantitative analysis of human CD8$^+$ T cells and IFN-γ in (D) and (F). Quantitative analysis of CD8$^+$ T and IFN-γ$^+$ using Aperio ImageScope software. (G) The infiltration of CD69$^+$ CD8 T cells in tumor tissues was identified using an anti-CD69 antibody (brown staining). (H) The statistical and quantitative analysis of (G). (I) The infiltration of TIM-3$^+$ CD8 T cells in tumor tissues was identified using an anti-TIM-3 antibody (brown staining). (J) The statistical and quantitative analysis of (I). The relative number of cells was calculated with Image-Pro-Plus. (K) H&E staining of tumor tissue sections. Scale bar = 50 μM. $^*P < 0.05$; $^{**}P < 0.01$; $^{***}P < 0.001$.

undergoing class switching and secreting human immunoglobulins in the sera of mice [39,40]. Human CD3$^+$CD4$^+$ and CD3$^+$CD8$^+$ T-cell subsets develop in both thymus-independent and thymus-dependent manners. In a thymus-independent manner, donor T cells expand in the periphery, similar to the expansion after PBMC injection [41,42]. Phenotypic analysis of thymocytes demonstrates that most T cells are produced in a thymus-dependent manner. In this way, a more diverse TCR repertoire can be presented, and no GvHD is found. Generally, there are three methods to identify the development of human thymus-dependent T cells [43]. First, TCR CDR3β

spectral typing is used to detect the diversity of the TCR library. Second, the expression of human TCRβ in T cells is quantified by TCR Cβ real-time PCR. Third, the TREC assay quantifies human sjTREC migrating from recent thymic cells [43]. Human T lymphoid precursor cells migrate with the blood circulation to the mouse thymus, undergo positive and negative selection under the induction of thymus hormone to obtain the restricted recognition ability of the major histocompatibility complex (MHC) and tolerance to self-antigens, and eventually develop into $CD4^+$ or $CD8^+$ T cells. The positive selection of human T lymphocytes relies on mouse MHC molecules. There may be a mismatch between mouse MHC and donor human leukocyte antigen (HLA), which will impair cellular immunity. Therefore, reconstruction of human T cells is more challenging than reconstruction of B cells in mice [38]. In this study, $CD3^+$ T cells were detectable at the 8th week, $CD3^+$, $CD4^+$, and $CD8^+$ T-cell subtypes were found in the peripheral blood at the 12th week, and the percentage of $CD8^+$ T cells was higher than that of $CD4^+$ T cells. $CD4^+$ T cells is commonly found in the early stage of T-cell development during the bone marrow transplantation process. Moreover, the differentiation of $CD8^+$ T cells occurs earlier than that of $CD4^+$ T cells [43]. Mounting evidence indicates that humanized NCG mice were successfully reconstructed by tail vein injection with $hCD34^+$ HSCs [11–13].

Next, we successfully constructed a CDX model in humanized mice. To verify whether this model could mimic the responses to immunotherapy and act as a platform for the evaluation of small molecule tumor immunotherapy drugs, we treated mice bearing HCT116 and SW480 tumors with BMS202. BMS202 has durable antitumour activity in both HCT116 and SW480 tumors. It achieves an antitumour immune response by activating recombinant human immune cells through PD-1/PD-L1 blockade. According to the flow cytometric analysis, the populations of $CD3^+$, $CD8^+$ and $CD8^+$ $IFN\gamma^+$ T cells were increased, whereas the Treg ($CD25^+FOXP3^+$) cells were decreased. The frequency of $CD8^+$ cytotoxic T cells and IFN-γ were increased significantly, while Ki67 expression was decreased. BMS202 shows a satisfactory antitumour response by blocking the PD-1/PD-L1 pathway and activating recombinant human T cells.

There are other difficulties in the exploitation of the humanized mouse model, including high cost and the appropriate time-point required for human immune cell reconstitution. It is necessary to further explore small animal models with lower cost and longer observation windows.

In summary, our findings indicated that (1) $hCD34^+$ HSCs are a good resource for the construction of humanized mouse models; (2) Radiation and tail intravenous injection are convenient and effective methods; and (3) the small molecule PD-1/PD-L1 checkpoint blocker BMS202 boosts antitumour responses in the hu-NCG colorectal cancer mouse model. $CD34^+$HSC-CDX NCG mouse models are appropriate preclinical models for studying immunological surveillance and immune modulation.

Supplementary Data

Supplementary data is available at *Acta Biochimica et Biophysica Sinica* online.

Funding

This work was supported by the grant from the National Natural Science Foundation of China (No. 81773028).

Conflict of Interest

The authors declare that they have no conflict of interest.

References

1. Malmberg KJ. Effective immunotherapy against cancer. *Cancer Immunol Immunother* 2004, 53
2. Kirkwood JM, Butterfield LH, Tarhini AA, Zarour H, Kalinski P, Ferrone S. Immunotherapy of cancer in 2012. *CA-Cancer J Clin* 2012, 62: 309–335
3. Sharma P, Allison JP. Immune checkpoint targeting in cancer therapy: toward combination strategies with curative potential. *Cell* 2015, 161: 205–214
4. Ribas A, Wolchok JD. Cancer immunotherapy using checkpoint blockade. *Science* 2018, 359: 1350–1355
5. Zitvogel L, Pitt JM, Daillère R, Smyth MJ, Kroemer G. Mouse models in oncoimmunology. *Nat Rev Cancer* 2016, 16: 759–773
6. Ngiow SF, Loi S, Thomas D, Smyth MJ. Mouse models of tumor immunotherapy. *Adv Immunol* 2016, 130: 1–24
7. Sanmamed MF, Chester C, Melero I, Kohrt H. Defining the optimal murine models to investigate immune checkpoint blockers and their combination with other immunotherapies. *Ann Oncol* 2016, 27: 1190–1198
8. Cheon DJ, Orsulic S. Mouse models of cancer. *Annu Rev Pathol Mech Dis* 2011, 6: 95–119
9. Okada S, Vaeteewoottacharn K, Kariya R. Application of highly immunocompromised mice for the establishment of patient-derived xenograft (PDX) models. *Cells* 2019, 8: 889
10. Olson B, Li Y, Lin Y, Liu ET, Patnaik A. Mouse models for cancer immunotherapy research. *Cancer Discovery* 2018, 8: 1358–1365
11. Choi B, Lee JS, Kim SJ, Hong D, Park JB, Lee KY. Anti-tumor effects of anti-PD-1 antibody, pembrolizumab, in humanized NSG PDX mice xenografted with dedifferentiated liposarcoma. *Cancer Lett* 2020, 478: 56–69
12. Chute JP, Muramoto G, Fung J, Oxford C. Quantitative analysis demonstrates expansion of SCID-repopulating cells and increased engraftment capacity in human cord blood following *ex vivo* culture with human brain endothelial cells. *Stem Cells* 2004, 22: 202–215
13. Giassi LJ, Pearson T, Shultz LD, Laning J, Biber K, Kraus M, Woda BA, *et al.* Expanded $CD34^+$ human umbilical cord blood cells generate multiple lymphohematopoietic lineages in NOD- *scid IL2r* γ^{null} mice. *Exp Biol Med (Maywood)* 2008, 233: 997–1012
14. Zhao Y, Shuen TWH, Toh TB, Chan XY, Liu M, Tan SY, Fan Y, *et al.* Development of a new patient-derived xenograft humanised mouse model to study human-specific tumour microenvironment and immunotherapy. *Gut* 2018, 67: 1845–1854
15. Morillon Ii YM, Sabzevari A, Schlom J, Greiner JW. The development of next-generation PBMC humanized mice for preclinical investigation of cancer immunotherapeutic agents. *Anticancer Res* 2020, 40: 5329–5341
16. Yaguchi T, Kobayashi A, Inozume T, Morii K, Nagumo H, Nishio H, Iwata T, *et al.* Human PBMC-transferred murine MHC class I/II-deficient NOG mice enable long-term evaluation of human immune responses. *Cell Mol Immunol* 2018, 15: 953–962
17. King MA, Covassin L, Brehm MA, Racki W, Pearson T, Leif J, Laning J, *et al.* Human peripheral blood leucocyte non-obese diabetic-severe combined immunodeficiency interleukin-2 receptor gamma chain gene mouse model of xenogeneic graft- *versus*-host-like disease and the role of host major histocompatibility complex. *Clin Exp Immunol* 2009, 157: 104–118
18. Lin S, Huang G, Cheng L, Li Z, Xiao Y, Deng Q, Jiang Y, *et al.* Establishment of peripheral blood mononuclear cell-derived humanized lung cancer mouse models for studying efficacy of PD-L1/PD-1 targeted immunotherapy. *mAbs* 2018, 10: 1301–1311
19. Wang M, Yao LC, Cheng M, Cai D, Martinek J, Pan CX, Shi W, *et al.*

Humanized mice in studying efficacy and mechanisms of PD-1-targeted cancer immunotherapy. *FASEB J* 2018, 32: 1537–1549
20. Tan S, Zhang CWH, Gao GF. Seeing is believing: anti-PD-1/PD-L1 monoclonal antibodies in action for checkpoint blockade tumor immunotherapy. *Sig Transduct Target Ther* 2016, 1: 16029
21. Hu Z, Yu P, Du G, Wang W, Zhu H, Li N, Zhao H, ***et al.*** PCC0208025 (BMS202), a small molecule inhibitor of PD-L1, produces an antitumor effect in B16-F10 melanoma-bearing mice. *PLoS ONE* 2020, 15: e0228339
22. Sasikumar PG, Ramachandra M. Small-molecule immune checkpoint inhibitors targeting PD-1/PD-L1 and other emerging checkpoint pathways. *BioDrugs* 2018, 32: 481–497
23. Zak KM, Grudnik P, Guzik K, Zieba BJ, Musielak B, Dömling A, Dubin G, ***et al.*** Structural basis for small molecule targeting of the programmed death ligand 1 (PD-L1). *Oncotarget* 2016, 7: 30323–30335
24. Weinmann H. Cancer immunotherapy: selected targets and small-molecule modulators. *ChemMedChem* 2016, 11: 450–466
25. Koboziev I, Jones-Hall Y, Valentine JF, Reinoso Webb C, Furr KL, Grisham MB. Use of humanized mice to study the pathogenesis of autoimmune and inflammatory diseases. *Inflammatory Bowel Dis* 2015, 21: 1652–1673
26. Benito AI, Diaz MA, González-Vicent M, Sevilla J, Madero L. Hematopoietic stem cell transplantation using umbilical cord blood progenitors: review of current clinical results. *Bone Marrow TransPlant* 2004, 33: 675–690
27. McDermott SP, Eppert K, Lechman ER, Doedens M, Dick JE. Comparison of human cord blood engraftment between immunocompromised mouse strains. *Blood* 2010, 116: 193–200
28. Vizzardelli C, Zimmann F, Nagl B, Kitzmüller C, Vollmann U, Gindl M, Tangermann S, ***et al.*** NSG mice humanized with allergen-specific T-cell lines as in vivo model of respiratory allergy. *Allergy* 2020, 75: 2081–2084
29. Greiner DL, Hesselton RA, Shultz LD. SCID mouse models of human stem cell engraftment. *Stem Cells* 1998, 16: 166–177
30. Park N, Pandey K, Chang SK, Kwon AY, Cho YB, Hur J, Katwal NB, ***et al.*** Preclinical platform for long-term evaluation of immuno-oncology drugs using hCD34$^+$ humanized mouse model. *J Immunother Cancer* 2020, 8: e001513
31. Choi B, Chun E, Kim M, Kim ST, Yoon K, Lee KY, Kim SJ. Human B cell development and antibody production in humanized NOD/SCID/IL-2Rγ null (NSG) mice conditioned by busulfan. *J Clin Immunol* 2011, 31: 253–264
32. Llewellyn GN, Alvarez-Carbonell D, Chateau M, Karn J, Cannon PM. HIV-1 infection of microglial cells in a reconstituted humanized mouse model and identification of compounds that selectively reverse HIV latency. *J Neurovirol* 2018, 24: 192–203
33. Seitz G, Pfeiffer M, Fuchs J, Warmann SW, Leuschner I, Vokuhl C, Lang P, ***et al.*** Establishment of a rhabdomyosarcoma xenograft model in human-adapted mice. *Oncol Rep* 2010, 24: 1067–1072
34. Heimfeld S. Bone marrow transplantation: how important is CD34 cell dose in HLA-identical stem cell transplantation? *Leukemia* 2003, 17: 856–858
35. Guo X, Yin X, Zhu W, Pan Y, Wang H, Liang Y, Zhu X. The preconditioning of busulfan promotes efficiency of human CD133$^+$ cells engraftment in NOD Shi-SCID IL2R gamma c null (NOG) mice via intra-bone marrow injection. *Cell TransPlant* 2019, 28: 973–979
36. Ito M, Hiramatsu H, Kobayashi K, Suzue K, Kawahata M, Hioki K, Ueyama Y, ***et al.*** NOD/SCID/γc null mouse: an excellent recipient mouse model for engraftment of human cells. *Blood* 2002, 100: 3175–3182
37. Hiramatsu H, Nishikomori R, Heike T, Ito M, Kobayashi K, Katamura K, Nakahata T. Complete reconstitution of human lymphocytes from cord blood CD34$^+$ cells using the NOD/SCID/γc null mice model. *Blood* 2003, 102: 873–880
38. Traggiai E, Chicha L, Mazzucchelli L, Bronz L, Piffaretti JC, Lanzavecchia A, Manz MG. Development of a human adaptive immune system in cord blood cell-transplanted mice. *Science* 2004, 304: 104–107
39. Billerbeck E, Barry WT, Mu K, Dorner M, Rice CM, Ploss A. Development of human CD4$^+$FoxP3$^+$ regulatory T cells in human stem cell factor–, granulocyte-macrophage colony-stimulating factor-, and interleukin-3-expressing NOD-SCID IL2Rγ null humanized mice. *Blood* 2011, 117: 3076–3086
40. Ishikawa F, Yasukawa M, Lyons B, Yoshida S, Miyamoto T, Yoshimoto G, Watanabe T, ***et al.*** Development of functional human blood and immune systems in NOD/SCID/IL2 receptor γ chain null mice. *Blood* 2005, 106: 1565–1573
41. Hesselton RM, Greiner DL, Mordes JP, Rajan TV, Sullivan JL, Shultz LD. High levels of human peripheral blood mononuclear cell engraftment and enhanced susceptibility to human immunodeficiency virus type 1 infection in NOD/LtSz-scid/scid mice. *J Infect Dis* 1995, 172: 974–982
42. Wagar EJ, Cromwell MA, Shultz LD, Woda BA, Sullivan JL, Hesselton RA, Greiner DL. Regulation of human cell engraftment and development of EBV-related lymphoproliferative disorders in Hu-PBL-*scid* mice. *J Immunol* 2000, 165: 518–527
43. Shultz LD, Lyons BL, Burzenski LM, Gott B, Chen X, Chaleff S, Kotb M, ***et al.*** Human lymphoid and myeloid cell development in NOD/LtSz- *scid IL2R* γ^{null} mice engrafted with mobilized human hemopoietic stem cells. *J Immunol* 2005, 174: 6477–6489